The Canadian Space Agency (CSA) Collision Risk Assessment and Mitigation System (CRAMS): Sharing the Development and the Operational Challenges.

Babiker Fathelrahman[1]; Doyon, Michel[2]; Abbasi Viqar[3];
Canadian Space Agency, Saint-Hubert, Quebec, J3Y 8Y9

The Canadian Space Agency has developed a multi-mission automated Collision Risk Assessment and Mitigation System (CRAMS). This paper describes the system and the challenges associated with its development and operation. The system receives e-mails and Conjunction Summary Messages (CSMs) from JSpOC, processes them and generates warning messages to the control centre when action is required based on predetermined thresholds. The system employs an approximate analytic probability model, and a conjunction geometry dependent hard body radius (HBR) for the primary object. The results of processing flight test data show accuracy extremely close to that of numerical integration in case of exact frame transformation. The limits of the simplifying assumptions for some transformations were also tested. To converge towards entry and exit (action –Stop action) criteria analysis was performed on past flight data and other data. The last challenge is the criterion on the quality of data given the fact that CSA receives only one or two data points before the time of conjunction. That implies that lack of sufficient data to test ability of covariance to predict miss distance variations for good quality data. One criterion was used for Radarsat-1 and Scisat based on not acting on any data of equivalent quality to that of TLEs. There has been previous decision not to act on TLE data after a visit and discussions with JSpOC.

[1] Flight Operation Analyst, CSA Satellite Operation, Space Utilization.
[2] Flight Operation Manager, CSA Satellite Operation, Space Utilization.
[3] Simulation Engineer, CSA Satellite Operation, Space Utilization.

I. INTRODUCTION

CSA received its first warning of a close approach between Radarsat-1 and two space objects from JSpOC through NORAD in 2005. CSA and JSpOC have interactively done the planning and the verification of the avoidance maneuver . Only the miss distances were provided then. In 2009 CSA started receiving warning e-mails with miss distance and radial error. It had to estimate the in-track and cross track errors from the radial to construct a collision avoidance box. In 2010 CSA started to receive e-mails with miss distances and the errors in radial, in-track and cross track axes and finally the CSMs.

In order to ensure that it is acting upon the best available information, CSA processes both the short-form email and the CSM. Due to satellite orbit information missing in the short-form emails, approximations are used to estimate the approach angle. Previously, CSA combined the error information for both satellites to construct a Collision Avoidance Box, and considered performing a collision avoidance maneuver if the situation was within the box. Since then, CSA has refined its methodology, implementing the Probability of Collision to get a more complete understanding of the risk involved in the close approach. Since the short-term email and the CSM have a well-defined format and structure, it was possible to automate the calculations. Thus, the CRAMS system automatically triggers as a result of incoming email and generates situational awareness data that is distributed to the appropriate operational teams almost instantly. The system is generic and robust enough to handle multiple missions that are operated at CSA, along with other missions, with no human intervention.

II. CRAMS DESCRIPTION

The CRAMS system has been operational since **November 2011**, supporting RADARSAT-1, RADARSAT-2 and SCISAT missions. Initially, the risk level was assessed primarily using the collision avoidance box. Since late 2011, the Probability of Collision calculations were incorporated into the system, along with a number of other improvements as a result of lessons learned. In 2012, the MOST spacecraft (operated by the University of Toronto's Space Flight Laboratory) was added to list of satellites for which CSA receives JSpOC notifications. CRAMS processes these notifications (CSM and short-form email) and distributes to the operational team at SFL. While MOST and SCISAT are not manoeuvrable spacecraft, an understanding of the threat to these satellites from space debris helps to understand the debris environment and plan mitigation strategies accordingly. In addition, if the close approach is with another operational satellite, avoidance operations could be coordinated with the other operators. Figure 1 shows the multi-mission operational context and interfaces of the CRAMS system.

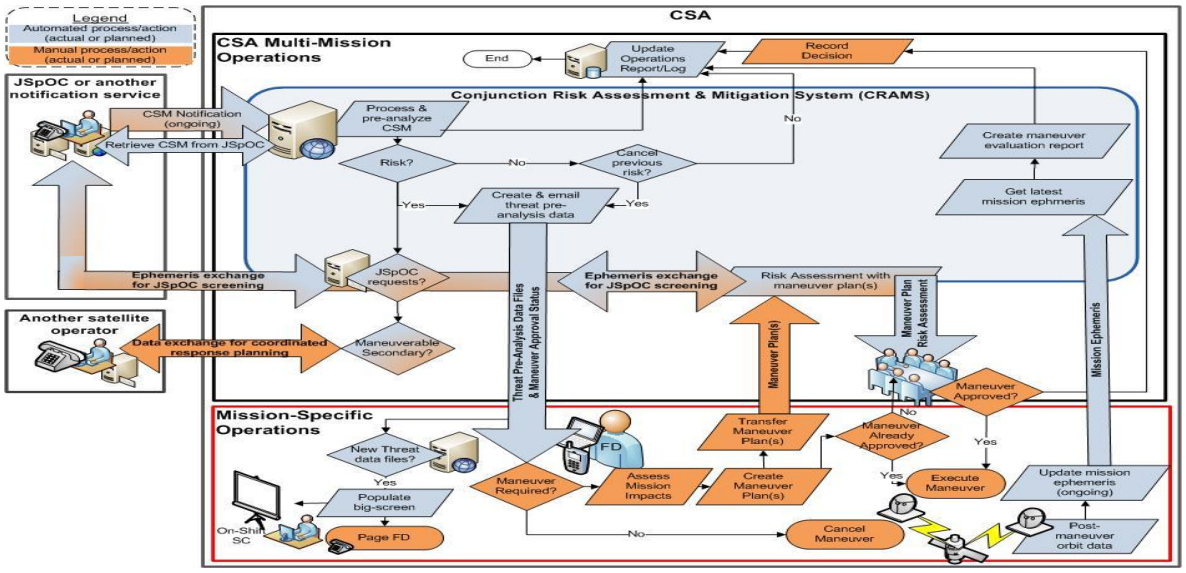

FIGURE 1. CRAMS BLOCK DIAGRAM

A. CRAMS INPUTS AND OUTPUTS

As shown in Figure 1, CRAMS processes JSpOC information and produces Threat Pre-Analysis data files, which include Risk Assessment data. Data is automatically emailed to a mission-specific distribution list. The data is compiled into a few formats: Excel spreadsheet, contains the original input data from JSpOC (email or CSM data), plus all the value-added content calculated in CRAMS, including graphics and charts. Summary text file, containing the most relevant information for operational decision-making from the original input data plus the value-added content, (no charts).XML output file, contains the original input data from JSpOC (email or CSM data), plus all the value-added content, minus graphics and charts. And STK scenario files

In current operations, only the Excel spreadsheet and summary text file are emailed to a mission-specific distribution list. The XML file and STK files stored on a network drive for review and analysis as necessary.

Plugging the position and velocity information from JSpOC, along with the covariance data for both objects, into STK, CRAMS automatically builds the STK scenario and executes the STK-based conjunction analysis tools (STK/AdvCAT). This generates an STK conjunction analysis report containing data, plus visualization of the scenario. The visuals – both a 2D and 3D view - are automatically incorporated into the Excel file to provide a quick, intuitive understanding of the pending situation in space.

III. CHALENGES

A. SELECTION OF PROBABILITY MODEL AND REQUIRED FRAME TRANSFORMATIONS

3.1.1Probability of Collision

3.1.1.1 Combined Covariance Matrix

Initially the approach angle was used to combine the two sets of uvw errors in order to have a single, representative set of errors to construct a collision avoidance box. This was refined later using the combined covariance [1,2]. For probability calculations, this process must be extended to the full covariance matrix that is provided in the CSMs..

Let the covariance matrices of the primary object and secondary object be C_p and C_s respectively each represented in their respective *uvw* coordinate systems, computed from the corresponding inertial position and velocity vectors. C_r represents the combined covariance matrix expressed in the UVW frame of the primary object.

To eliminate the errors associated with the transformations using the approach angle, a more precise transformation can be implemented. The state vector (position and velocity) of each objects (primary and secondary) is transformed into Earth Centered Inertial (ECI) coordinates. It is then used to define transformation matrices (direction cosine) from the primary and secondary frames and to transform the primary and secondary covariances in ECI coordinates. Subsequently, the relative position covariance (in ECI) is obtained by adding the two covariance matrices. Finally, the combined covariance matrix is converted back to the primary frame (*(u,v,w)* of the primary). The approach is as follows. First, convert the R and V primary and secondary vectors from the EFG to the ECI frame (2 each, for a total of 4 transformations).

, transformation matrices, T_p and T_s, can be created using $\vec{r_p}$, $\vec{v_p}$, $\vec{r_s}$, $\vec{v_s}$ in the ECI frame such that

$$\boldsymbol{T_p} = \begin{bmatrix} \hat{\boldsymbol{u}}_{\boldsymbol{p}} \\ \hat{\boldsymbol{v}}_{\boldsymbol{p}} \\ \hat{\boldsymbol{w}}_{\boldsymbol{p}} \end{bmatrix} \tag{1}$$

Where $\hat{u}_p$, $\hat{v}_p$, and $\hat{w}_p$, are the unit vectors of the primary spacecraft in the *uvw* frame defined by its ECI position vector. The $\hat{u}_p$ vector is defined as a unit vector in the direction of the ECI object position vector from the center of the Earth to the spacecraft and calculated as follows:

$$\hat{\boldsymbol{u}}_{\boldsymbol{p}} = \overrightarrow{\boldsymbol{r_p}} \Big/ \left|\overrightarrow{\boldsymbol{r_p}}\right| \tag{2}$$

The cross-track component, $\hat{w}_p$, is defined by the cross product of the ECI radial and velocity vectors:

$$\hat{\boldsymbol{w}}_{\boldsymbol{p}} = \overrightarrow{\boldsymbol{r_p}} \times \overrightarrow{\boldsymbol{v_p}} \Big/ \left|\overrightarrow{\boldsymbol{r_p}} \times \overrightarrow{\boldsymbol{v_p}}\right| \tag{3}$$

And, finally, the in-track component completes the triad.

$$\hat{\boldsymbol{v}}_{\boldsymbol{p}} = \hat{\boldsymbol{w}}_{\boldsymbol{p}} \times \hat{\boldsymbol{u}}_{\boldsymbol{p}} \tag{1}$$

The transformation matrix for the secondary object is similarly constructed:

$$\boldsymbol{T_s} = \begin{bmatrix} \hat{\boldsymbol{u}}_{\boldsymbol{s}} \\ \hat{\boldsymbol{v}}_{\boldsymbol{s}} \\ \hat{\boldsymbol{w}}_{\boldsymbol{s}} \end{bmatrix} = \begin{bmatrix} \overrightarrow{\boldsymbol{r_s}} \Big/ |\overrightarrow{\boldsymbol{r_s}}| \\ \hat{\boldsymbol{w}}_{\boldsymbol{s}} \times \hat{\boldsymbol{u}}_{\boldsymbol{s}} \\ \overrightarrow{\boldsymbol{r_s}} \times \overrightarrow{\boldsymbol{v_s}} \Big/ |\overrightarrow{\boldsymbol{r_s}} \times \overrightarrow{\boldsymbol{v_{sp}}}| \end{bmatrix} \tag{5}$$

From that, the primary and secondary covariance matrices can be transformed into the ECI frame:

$$\boldsymbol{C_{pECI}} = \boldsymbol{T_p^T}\, \boldsymbol{C_{puvw}}\, \boldsymbol{T_p} \tag{6}$$

6

$$\boldsymbol{C_{sECI}} = \boldsymbol{T_s^T}\, \boldsymbol{C_{suvw}}\, \boldsymbol{T_s} \tag{7}$$

And the combined covariance for the encounter is the sum of the above two matrices.

$$\boldsymbol{C_{rECI}} = \boldsymbol{C_{pECI}} + \boldsymbol{C_{sECI}} \tag{8}$$

Finally, C_r in the UVW frame of the primary object is given by:

$$C_r = \boldsymbol{C_{ruvwp}} = \boldsymbol{T_p}\, \boldsymbol{C_{rECI}}\, \boldsymbol{T_p^T} \tag{9}$$

3.1.2 *PROBABILITY CACULATION*

While methods have been presented above to determine a level of severity to the spacecraft given limited information (such as DOI) when the full information of the JSpOC CSM is unavailable, a more thorough method of determining the severity of the event to the health and safety of the spacecraft is desirable. The metric that is most commonly used is the so-called "probability of collision". Klinkrad[1] has provided a very thorough discussion of the measure of the probability of spacecraft collision and the descriptions below are based on [Ref.1 The more theoretical background can be obtained from [Ref.1 as well as Ref.2.

The equation below represents the generalized expression of probability. It represents the integration of the probability density function over the volume. In its un-modified form, it is used for long encounter durations (*i.e.* minutes).

$$\boldsymbol{P} = \frac{1}{\sqrt{(2\pi)^3 |\boldsymbol{C}|}} \iiint_{\boldsymbol{V}} \boldsymbol{e}^{-\frac{1}{2}\boldsymbol{r}^T \boldsymbol{C}^{-1} \boldsymbol{r}}\, \boldsymbol{dxdydz} \tag{10}$$

However, for short encounters, it can be reduced to a 2-D problem. This is based on the assumption of rectilinear motion in the encounter region. In this case, the probability value is independent of the error in the direction of the relative velocity vector.

To simplify this equation, an encounter coordinate system (*x*,*y*,*z*) is defined at the time of closest approach (TCA) such that the origin is taken to be one of the two objects The *x*-axis is along the miss distance vector $\vec{r}$, the *y*-axis is along the relative velocity vector $\overrightarrow{v_r}$, and the *z*-axis along $\vec{r} \times \overrightarrow{v_r}$. The *xz* plane defines the encounter plane (also called the B-plane). In the encounter plane, the most significant contribution comes from the error component along the miss distance. Figure 2[2] shows the geometry of the encounter plane.

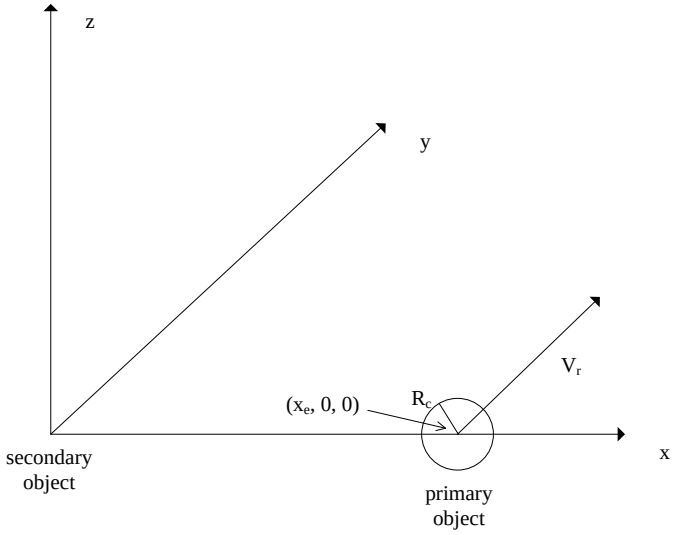

Figure 2. Encounter Plane Geometry

The equation below is the simplified, two-dimensional equation resulting from Equation 32 above. It is implemented in STK/CAT using two different approaches to approximate the double integral: a numerical one[3] and analytical ones. [2,4]

$$\boldsymbol{P} = \frac{1}{2\pi\sigma_x\sigma_z\sqrt{1-\rho_{xz}{}^2}} \iint_A \boldsymbol{e}^{\frac{-\left[\left(\frac{x}{\sigma_x}\right)^2 - 2\rho_{xz}\left(\frac{x}{\sigma_x}\right)\left(\frac{z}{\sigma_z}\right) + \left(\frac{z}{\sigma_z}\right)^2\right]}{2(1-\rho_{xz}{}^2)}} \boldsymbol{dxdz} \qquad (11)$$

The above equation is not readily solvable, so a simplified solution is desired to allow for rapid processing independent of COTS software. The following sections describe two analytical methods to solve the two-dimensional probability equation above.

3.1.3 ENCOUNTER FRAME APPROACH

The main assumption is that the variation of the probability density function is insignificant within the encounter region, i.e. a constant density. We have from Ref2.

$$\boldsymbol{P_{appr}} = \frac{R_c{}^2}{2\sigma_x\sigma_z\sqrt{1-\rho_{xz}{}^2}} \boldsymbol{e}^{\frac{r^2}{-2\sigma_x{}^2(1-\rho_{xz}{}^2)}} \qquad (12)$$

In the above equation, r is the miss distance between the two objects.

In order to implement (12), the following transformations are necessary for transforming the data in the form appropriate for use in the probability formula.

In the encounter plane, the assumption of linear motion is valid for short encounters (duration of seconds) typical for LEO encounters. An encounter coordinate system is defined where the unit vectors are as follows. The x-axis is taken to be the miss distance vector as defined by:

$$\hat{\boldsymbol{x}} = \frac{\vec{\boldsymbol{r}}}{|\vec{\boldsymbol{r}}|} = \left(\frac{\boldsymbol{u}}{\sqrt{\boldsymbol{u^2+v^2+w^2}}} , \frac{\boldsymbol{v}}{\sqrt{\boldsymbol{u^2+v^2+w^2}}} , \frac{\boldsymbol{w}}{\sqrt{\boldsymbol{u^2+v^2+w^2}}} \right) = (\boldsymbol{n_1}, \boldsymbol{n_2} , \boldsymbol{n_3}) \tag{13}$$

The y-axis is taken as the direction of the relative velocity vector:

$$\hat{\boldsymbol{y}} = \frac{\overrightarrow{\boldsymbol{v_r}}}{|\overrightarrow{\boldsymbol{v_r}}|} = (\boldsymbol{p_1}, \boldsymbol{p_2} , \boldsymbol{p_3}) \tag{14}$$

And the z-axis completes the triad:

$$\hat{\boldsymbol{z}} = \frac{\vec{\boldsymbol{r}} \times \overrightarrow{\boldsymbol{v_r}}}{|\vec{\boldsymbol{r}} \times \overrightarrow{\boldsymbol{v_r}}|} = (\boldsymbol{q_1}, \boldsymbol{q_2} , \boldsymbol{q_3}) \tag{2}$$

From the above, the transformation matrix, T_{xyz}, to rotate the relative covariance matrix (where $C_r = C_{pECI} + C_{sECI}$) in the primary uvw frame to the relative position covariance matrix C in the encounter frame is as follows:

$$\boldsymbol{T_{xyz}} = \begin{bmatrix} \boldsymbol{n_1} & \boldsymbol{n_2} & \boldsymbol{n_3} \\ \boldsymbol{p_1} & \boldsymbol{p_2} & \boldsymbol{p_3} \\ \boldsymbol{q_1} & \boldsymbol{q_2} & \boldsymbol{q_3} \end{bmatrix} \tag{16}$$

And the transformation of the covariance matrix is as follows:

$$\boldsymbol{C_{xyz}} = \boldsymbol{T_{xyz}}\, \boldsymbol{C_r} \boldsymbol{T_{xyz}}^{\boldsymbol{T}} = \begin{bmatrix} \boldsymbol{\sigma_x}^{\boldsymbol{2}} & \boldsymbol{\sigma_{xy}} & \boldsymbol{\sigma_{xz}} \\ \boldsymbol{\sigma_{xy}} & \boldsymbol{\sigma_y}^{\boldsymbol{2}} & \boldsymbol{\sigma_{yz}} \\ \boldsymbol{\sigma_{xz}} & \boldsymbol{\sigma_{yz}} & \boldsymbol{\sigma_z}^{\boldsymbol{2}} \end{bmatrix} \tag{17}$$

Within the encounter coordinate frame, there is an "encounter plane" which is defined as the plane perpendicular to the velocity vector. Since the velocity vector is along the y-axis, this is therefore referred to as the "*xz*" plane.

T_{xz} is a matrix that transforms the relative position covariance matrix C_{r} in the $u_p v_p w_p$ frame to the *xz* frame on the encounter plane to produce the 2-D covariance matrix C_{xz}. It is defined as follows:

$$\boldsymbol{T_{xz}} = \begin{bmatrix} \boldsymbol{n_1} & \boldsymbol{n_2} & \boldsymbol{n_3} \\ \boldsymbol{q_1} & \boldsymbol{q_2} & \boldsymbol{q_3} \end{bmatrix} \tag{18}$$

And the covariance matrix in the 2-D encounter plane is given by:

$$\begin{aligned} \boldsymbol{C_{xz}} &= \boldsymbol{T_{xz}}\, \boldsymbol{C_r} \boldsymbol{T_{xz}}^{\boldsymbol{T}} \\ &= \begin{bmatrix} \boldsymbol{\sigma_x}^{\boldsymbol{2}} & \boldsymbol{\sigma_{xz}} \\ \boldsymbol{\sigma_{xz}} & \boldsymbol{\sigma_z}^{\boldsymbol{2}} \end{bmatrix} \\ &= \begin{bmatrix} \boldsymbol{\sigma_x}^{\boldsymbol{2}} & \boldsymbol{\rho_{xz}\sigma_x\sigma_z} \\ \boldsymbol{\rho_{xz}\sigma_x\sigma_z} & \boldsymbol{\sigma_z}^{\boldsymbol{2}} \end{bmatrix} \end{aligned} \tag{19}$$

where

$$\boldsymbol{\rho_{xz}} = \frac{\boldsymbol{\sigma_{xz}}}{\boldsymbol{\sigma_x\sigma_z}} \tag{20}$$

Alternatively the above analysis can be extended as in Ref.1 and Ref.2 using the eigen values and eigen vectors to finally derive Eqs 21 and 22.

$$\boldsymbol{P} = \frac{1}{2\pi\sigma_{x}{}'\,\sigma_{z}{}'} \iint_{A} \boldsymbol{e}^{\frac{-1}{2}\left[\left(\frac{x'^{2}}{\sigma_{x}{}'^{2}}\right)+\left(\frac{z'^{2}}{\sigma_{z}{}'^{2}}\right)\right]}\, \boldsymbol{dx'dz'} \tag{21}$$

This has the approximate solution given by:

$$\boldsymbol{P_{appr}} = \frac{R_c^2}{2\sigma_X'\sigma_Z'}\exp\left\{-\frac{1}{2}\left[\left(\frac{r\cos\varphi}{\sigma_x{}'}\right)^2+\left(\frac{r\sin\varphi}{\sigma_z{}'}\right)^2\right]\right\} \tag{22}$$

The approximate probability formula is known to follow closely the numerically computed probability in the ranges of operational interest as reported in Ref. 5.

3.1.4 HARD BODY RADIUS

As can be seen in Es 12 and(22 the probability result is directly proportional to the square Hard Body Radius (HBR) used. This makes the definition of this parameter a critical one in determining an accurate measure of the probability of collision.

Typically, the cross-sectional size of the primary object is well known. For example, the effective hard body radius of RADARSAT-1 is either 7.5m or 2.0m depending on the side observed. If observed from the side (approach angle of 90º) the total length of the spacecraft is 15 m. If observed from the front (approach angle of 180º), the total height of the spacecraft is 4 m.

The following formula gives a close approach geometry dependent HBR for RADARSAT-1 and RADARSAT-2 (which have similar geometries).

$$HBR = 2m\,cos\gamma + 7.5m\sin\gamma \tag{23}$$

Where γ is the angle between the relative velocity vector ($\overrightarrow{V_r}$) and the $\hat{v}$-axis of the primary object. It is defined by:

$$\gamma = acos\left(abs\left(\frac{\overrightarrow{V_r}}{|\overrightarrow{V_r}|}\cdot -\hat{v}\right)\right) \tag{24}$$

Where $\hat{v}$ is defined in Eq. 4, and $\overrightarrow{V_r}$ is the relative velocity vector.

For SCISAT-1 a static HBR of 0.56 m is used, as its more compact nature lends itself more to an approximation of a sphere.

For the secondary object, depending on the information provided by the CSM, the hard body radius will be based on the measured cross-section and referenced from the following table.

Default values for the HBR of the secondary object are derived from the JSpOC CSM (small < 0.1 m^2, medium 0.1 m^2 < x < 1 m^2, large > 1 m^2) and are inspired from ESOC's approach to give a minimum HBR of 1 m to secondary objects. This is an open issue to be resolved considering the gravity gradient orientation of a lot space debris.

Also, depending on the secondary object, additional information may be available from various sources. The combination of the hard body radius for the secondary object and the result of Equation (50) provides the value for R_C in the probability equations.

Historically, a safety factor of 50m around the objects was used when using a Box approach. This is no longer required when using probability and the dimensions of the objects (radius) are used (7.5m for RADARSAT-1 and RADARSAT-2, 0.56m for SCISAT-1).

B. VALIDATION OF PROBABILITY CALCULATION

The implementation was compared with test cases evaluated by experts from 8 different organizations. These results are summarized in Ref. 6and show good comparisons for a single event.

In order to expand on the results from various comparisons with other systems computing probability have been conducted. The table below presents some of the results of a number of close approach events by comparing CRAMS with digitally computed probabilities .

Table 1. Probability comparison results

Event	Primary Object HBR (m)	Secondary Object HBR (m)	CRAMS Probability	Probability-digitalyl integ-1	Probability-digitally integ-2
2011-09-07--R1-COSMOS_2251_DEB_csm201124826099	2.1	1.0	2.268E-05	2.055E-05	2.043E-05
2011-08-20--R2-DELTA_2_RB_csm201123024856	7.5	2.985	0.0	1.000E-30	0.0
2011-08-05--R2-COSMOS_2251_DEB_csm201121523811	7.5	1.0	1.5725E-11	4.807E-11	4.769E-11
2011-08-05--R2-COSMOS_2251_DEB_csm201121423764	7.5	1.0	3.2735E-10	6.426E-10	6.353E-10
2011-07-27--S1-CZ-4_DEB_csm201120523214	0.55	1.0	1.0521E-12	1.078E-12	1.070E-12
2011-06-30--R2-COSMOS_2251_DEB_csm201118021655	7.5	1.0	5.929E-60	1.000E-30	1.189E-59
2011-06-21--R1-IRIDIUM_33_DEB_csm201117021052	2.1	1.0	2.6611E-05	2.707E-05	2.690E-05
2011-06-15--R1-SL-3_RB_csm201116620764	2.1	1.9	0.0	1.000E-30	0.0
2011-05-25--R2-COSMOS_2251_DEB_csm201114319494	7.5	1.0	7.581E-03	7.695E-03	7.647E-03

The above table shows that there is very good agreement between the probabilities as implemented in CRAMS and digitally integrated probabilities

Table 2. CRAMS and digitally integrated Probabilities

Case ID	STK (Alfano)	UVW	ECI	Organization1	Approach Angle
1	4.1353e-005	8.8603e-005	6.1943e-005	8.8363e-005	119.5
2	2.3544e-006	2.025e-019	2.3577e-006	5.2919e-007	44.9
3	9.8557e-006	1.2333e-005	9.8298e-006	2.0047e-006	71.0
4	4.7409e-005	7.2415e-005	5.0817e-005	7.2432e-005	11.3
5	1.7301e-005	1.9326e-005	1.7252e-005	1.9604e-005	71.1
6	4.1983e-005	1.6388e-005	4.0082e-005	1.0869e-005	80.1

As can be seen fromTables 1 and 2 there is good agreement between the CRAMS data sets and organization1 data. In particular the UVW data tracks very closely with other agencies results. It is likely that this is how they transform their covariance matrices for calculating probability. The ECI results are not significantly different from these other two sets of results, and they track very well with the STK results. Given that there are known approximations in the UVW approach and that the ECI transformation is a more rigorous method, the differences are not entirely unexpected. The overall correlation between the various data sets does lead to the conclusion that the CRAMS probabilities are being accurately calculated.

C. IMPLEMENTATION

Both the eigen and non-eigen methods for probability calculation have been implemented and lead to the same results.

Following Eumetsat work, a weighted average of 3 values of probability evaluated at the centre, at +HBR/2 and at –HBR/2 is also implemented.

CRAMS will have the ability to calculate probability based on these alternate methods but the method based on Eq. 12 will be used operationally as it is more robust.

D. ENTRY AND EXIT CRITERIA

A probability of collision greater or equal to 1.0e-04 represents the action criteria. This number has extensive operational heritage with other missions, including use by the Space Test Squadron (Air Force Space Command Collision Avoidance process); it is also detailed in NASA's Orbital Debris Conjunction Assessment and Collision Avoidance Strategy; and in Ref. 7 .

A post-manoeuvre exit criterion is not nearly as well agreed upon and requires some measure of analysis. One method to determine the valid exit criterion would be to target a miss distance of at least $3\sigma_x' cos\varphi$ to get out of the projected relative position covariance ellipse on the encounter plane which should drive the probability towards zero as elaborated in Ref. 8. However, the drawback of using this method is that it is not consistent with the methods of determining when to perform a manoeuvre in the first place (*i.e.* probability). In order to understand better the relationship between this threshold value and probability, a series of CSMs obtained from Space-Track.org was processed to determine the approximate probability of collision for each event. Only events that had a probability of greater than 1E-04 are presented here. Additionally, for each event, the $3\sigma_x' cos\varphi$ value was determined as the final miss distance, and the probability calculated from that. Both the initial probability (red squares) and the threshold probability (blue diamonds) are plotted below for each event.

As can be seen, the threshold probability associated with $3\sigma_x' cos\varphi$[8] is not constant from event to event. This is likely due to the fact that the covariances are not constant, but vary from event to event as well. There is a

trend towards numbers generally below 1E-05 with the lowest two between 1E-11 and 1E-13 . If one looks, however, at where most of the "Exit" data is plotted, one can see that the data generally is above 1E-09. From this plot it would be reasonable to use 1E-09 as the exit criteria for burn planning based on the $3\sigma_x^{'}cos\varphi$ threshold. In addition, 1E-09 is referenced in Ref. 7as the criterion for a successfully sized manoeuvre.

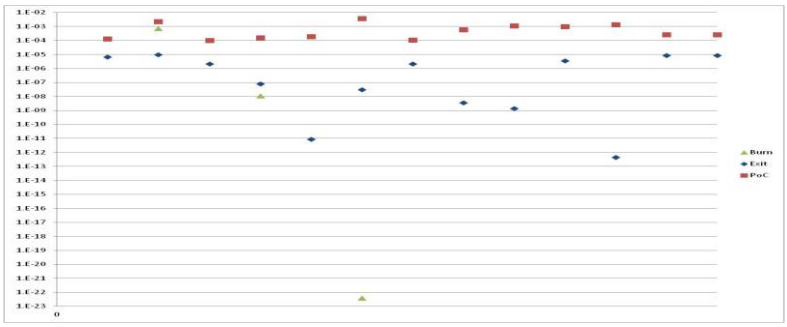

Figure III-1 Exit criteria based on encounTer plane geometry

Also plotted, are green triangles which show the approximate probability for three actual escape manoeuvres performed for this data set. Of these three events, one burn would not have exceeded the "exit criteria". In fact, that one burn (the first of the three in the above plot) was not even large enough to create a < 1E-04 probability of collision. However, the other two were large enough that if the $3\sigma_x^{'}cos\varphi$ value were used as a criterion, the burns would have been large enough to pass this criterion. One would have achieved a 1E-08 probability, and the other ~1e-22.

It is clear that the previous method of sizing burns (escape from a collision avoidance box created based on location errors) is not consistent with a probability-based exit criterion. This does not specifically cast doubt on either method, but it does show that there is no one "correct" method for determining when a situation is "safe". The goal here in choosing a probability exit criterion is to maintain consistency in how one defines a high and low risk situation.

E. IMPACT OF MANOEUVRE ON COVARIANCE MATRIX

Once it has been decided that the probability of collision is high enough that an escape manoeuvre is warranted, the effect on the probability of collision by the new displacement as well as by the error induced by uncertainty in the burn must be considered.

The new location of the spacecraft at TCA can be determined via the CW equations[9], and the new miss distance can be evaluated as in Ref. 10 .

If it were the case that the requested manoeuvre size had zero error with respect to the actual delivered change in velocity, the probability can be calculated with the original covariances and the new close approach vector. This assumes that the original covariances are constant over the region of space that includes the original close approach location and the new time of closest approach. However, the manoeuvre itself carries with it some uncertainty, so that must be factored into the probability.

We make use of the assumptions above, that the covariances of the locations of the two objects are not changed due to the change in location and the change in the time of closest approach. Additionally, it is assumed that the error in the change in velocity is an independent source of error. Therefore, the final covariance of the primary object (the one assumed to be manoeuvring) is simply a summation of the original covariance and the error in the change in velocity.

Indicating that the error in the change in velocity is directly proportional to the error in the final in-track location as the change in velocity is to the change location.

In a routine RADARSAT-1 manoeuvre, the worst case observed error for an in-track manoeuvre, ε_m, is 5% of the change in velocity. (In actuality, the error observed is the error in the change in semi-major axis of the manoeuvre, but this is proportional to the change in velocity[7].

Substituting the sigma value of 5% (R1 maximum error in the worst case, i.e. 3 sigma error) we have:

$$\sigma^2_{v(t)} = 0.0025\, t^2 \dot{v_0}^2 \text{ (Refs. 7,9)} \qquad (25)$$

The covariance is then simply added to the initial covariance of the primary object at the time of closest approach to arrive at a new, burn-induced covariance. The probability is calculated as in the pre-burn case but with the new post-manoeuvre covariance. Note that the values for the covariances due to the manoeuvre in the radial and cross-track are assumed to be zero.

It should be noted that an in-track change in velocity does induce a radial change in the location of the satellite along the orbit. Specifically, for a single thrust at a single point in the orbit, the radial position will be changed such that it is maximized at the opposite side of the orbit as the manoeuvre and minimized (actually is 0) at the point in the orbit that the manoeuvre occurs. However, these changes in radial position are small and are constant unlike the changes in the in-track position which are significant larger and build up over time. For the purposes of this analysis they are ignored.

G. DATA QUALITY Indicators

3.7.1 TLE QUALITY AS THE LIMIT FOR SP DATA QUALITY

The level of measurement errors, the level of orbit prediction and determination errors in the data received from JSpOC may lead to erroneous or misleading results when computing probability or D Prior to the advent of the JSpOC notification system currently in place, the only method of determining whether close approach events were to occur was by comparing the widely available TLEs that are disseminated for the known objects in low-Earth orbit. However, it has since become evident that the errors on these vectors are much too large to effectively generate believable close approach events.

At the CSM workshop in October 2010 (, estimates for TLE prediction were presented for 18 and 72 hours prediction cases[11]. In the case of CSA spacecrafts (LEO altitude > 500km),

In order to determine the impact of these values on the previous analyses, the below plot is presented. It shows the In-track 1-sigma error from a series of 60+ CSMs, with the blue line. Superimposed on this line, are orange diamond markers which indicate which of these events had resulting probabilities of greater than 1E-04, the previously proposed threshold for determining whether an event requires an escape manoeuvre. (They are, in this case, simply Boolean markers; they do not represent a value on a scale.) Finally, the red line represents the above 72 hours TLE prediction error. (The assumption is that the majority is in the in-track direction for this plot, when in reality it is RSS.

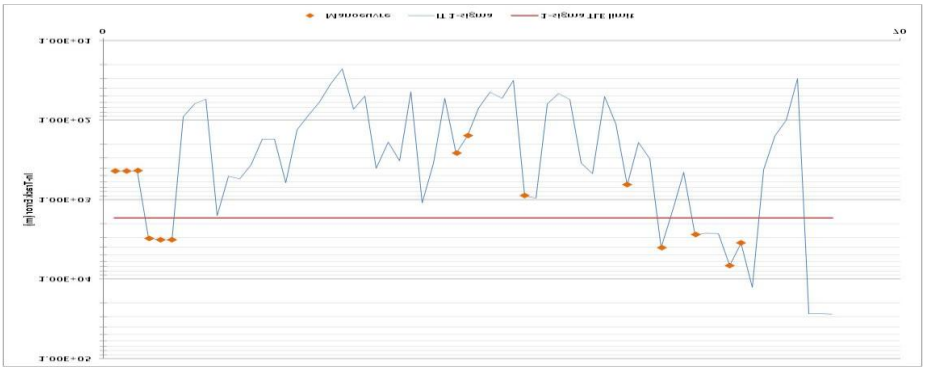

Figure III-2 In-track Errors compared to TLE ERROR Limits

The primary information to take away from this plot is that there are several events (7 in the above sampling) that would be defined as requiring a manoeuvre, but with in-track errors that exceed the known magnitude for TLE errors. For this reason, it is recommended here that a limit on the magnitude of measured errors by JSpOC

be imposed prior to deciding on whether to perform a manoeuvre. This limit would be the limit of TLE RSS errors, propagated to 72 hours, and would be imposed on both primary and secondary objects. If either of the two objects were to violate the limit of 1.7km, no decision would be made until the errors were reduced to a lower level.

3.7.2 CSM QUALITY INDICATORS

CSM Data: these are: how recent the data are, the data arc with respect to the optimum arc, and the number of data points used in orbit determination are OD quality indicators available in the CSM.

3.7.3 DATA CONSISTENCY

When you have more than one CSM the ability of the previous covariance to predict the recent one gives a measure of data consistency. But if there only one covariance before the close approach then that measure is lacking and the use of a cut-ff limit on RSS error of the SP data as the TLE is a reasonable alternative.

H. TIMELY PRODUCTION OF A MANEUVER TRADE SPACE

In the situation where a close approach alert leads to a manoeuvre, a manoeuvre trade space is required to provide options within the close approach and system constraints that enables the selection of the optimum avoidance manoeuvre for increasing the separation distance and reducing the risk of collision to an acceptable level (e.g. 5 orders of magnitudes lower than 1.0e-04). Software such as STK Astrogator and CAT allow computing a manoeuvre trade space based on the information provided by the CSM information. Such calculation is computer intensive and requires the use of expensive software. McKinley[10] presents a simplified method allowing fast calculation of sufficient level of accuracy following an analytic approach rather than the numeric approach employed in an older version of CRAMS using STK Astrogator and CAT and tools similar to it. This analytic approach has been implemented in-house and tested.CRAMS produces a number of maneuver trade space charts. In addition to the charts, the data is also available in table form.

.

ACKNOWLEDGMENTS

In the writing of this paper and the development of the associated operational tools, we would like to acknowledge the feedback and information provided by various space agencies and satellite operators. Their feedback was instrumental in allowing us to develop our expertise in a short period of time. Namely, we would like to recognize ESA-ESOC, EUMETSAT, CNES, AFSPC and the Joint Space Operations Command (JSpOC).

REFERENCES

[1] Klinkrad, Heiner, *Space Debris Models and Risk Analysis*, PARAXIS PUBLISHING Ltd, Chucgdster,UK, 2006, chap 8

[2] Chan, Kenneth, *Spacecraft Collision Probability*, The Aerospace Press, El Segundo , California, 2008, chap 1-6.,2008

[3] Alfano, Salvatore A Numerical Implementation of Spherical Object Collision Probability, The Journal of Astronautical Sciences - Jan – Mar 2005

[4] Patera, R. P. General Method for Calculating Satellite Collision Probability, AIAA Journal of Guidance, Control, and Dynamics Vol 24, No 4. July – August, 2001

[5]Alfriend, K. et al. Probability of Collision Error Analysis - 1999
[6]Wysack, Joshua, et al. The JAXA report (Agency probability comparison methods) - 2010, 2011

[7] Righetti, Pier Luigi et al. Handling of conjunction warnings in Eumetsat Flight Dynamics - -
[8]Frigm, Ryan C. et al. Assessment , Planning & Execution considerations for Conjunction Risk Assessment and Mitigation Operations, SpaceOps 2010 - 2010

[9]Cliff, Eugene M. Clohessey-Wiltshire Analysis Oct 23, 1998
[10]McKinley, David *Manoeuvre Planning for Conjunction Risk Mitigation with Ground Track Control Requirements*

[11] Kaya, Denise & Ericson, Nancy JSpOC/ESA post conjunction event analysis - Oct 2010 - -